Field Ionization and Field Emission
with Intense, Single-cycle THz Pulses
Need to replace with my own title

by

© Yunxiao Wang

A thesis submitted to the

School of Graduate Studies

in partial fulfilment of the

requirements for the degree of

Anqing, Anhui, China

B.S. in Physics University of Science and Technology of China May 2009

Memorial University of Newfoundland

Doctor of Philosophy

St. John's   Newfoundland

Department of Physics August, 2016

Abstract

Nuclear-polarized ^{3}He targets have been widely used in electron-scattering experiments in Thomas Jefferson National Accelerator Facility (JLAB) since mid 1990s. It is of great importance to produce large amounts of ^{3}He gas with high polarization.

The latest experiments run in JLAB prior to the 12GeV upgrade have been using cells polarized with Spin-Exchange Optical Pumping (SEOP). These cells were made of the GE180 glass and use a two-chambered design. The top chamber, known as the pumping chamber, is where ^{3}He is polarized through SEOP. The bottom chamber, known as the target chamber, is where electron scattering occurs. Great effort has been made in our lab to develop this generation of cells. Alkali-hybrid SEOP together with narrowband laser diode arrays have increased the ^{3}He polarization from 37% to 65%. Among other things, we also carefully studied an additional spin relaxation mechanism that limits the maximum achievable ^{3}He polarization.

The 12GeV upgrade makes the future experiments much more demanding in terms of target cell performance. One challenge it brings is the high relaxation due to electron beam. We have designed and tested a new style cell that uses convection instead of diffusion to increase the rate at which the polarization in the target chamber is being replenished by gas from pumping chamber. We have obtained over 50% polarization with controllable convection speed so far.

An additional problem that comes with higher beam current is that the glass end windows of traditional design are not likely to survive the experiments. Our group started exploring the option of using metal end windows from a decade ago. The first problem to solve is to find out the correct material and the proper technique

to incorporate metal without introducing significant spin relaxation and still being able to hold high pressure gas (12 atm) inside. This is a brand new technique that may have a profound impact of future cell designs once fully developed. Although no metal end windows have been tested so far, multiple glass cells with different kinds metal tubes (much larger in area compared to the end windows that will be used in JLAB experiments) attached were examined and were enough to convince us the extra spin relaxation is not likely to cause significant problems. The metals tubes were connected to Pyrex glass with knife-edge (housekeeper) seals and stayed intact through high pressure tests. After exploring options such as pure copper, gold coated copper, titanium, stainless steel, gold coated titanium, we have established that electroplating gold on copper substrate yields the best result so far. Further tests are planned before attaching metal end windows to GE180 glass and using them in electron-scattering experiments.

Acknowledgements

Put your acknowledgements here...

"Intellectual and practical assistance, advice, encouragement and sources of monetary support should be acknowledged. It is appropriate to acknowledge the prior publication of any material included in the thesis either in this section or in the introductory chapter of the thesis."

— MUN School of Graduate Studies

Contents

List of Tables

List of Figures

Chapter 1

Spin-Exchange Optical Pumping

1.1 Overview

Spin-polarized noble gases have been widely used for various purposes. In JLAB, polarized ^{3}He is used as target for electron-scattering experiments. This is because a ^{3}He nucleus has a pair of protons with paired spins and a single neutron that contributes the most of the nuclear spin. In MRI, polarized ^{3}He has seen uses such as detecting structural damage in the lungs.

There are generally two ways of polarizing ^{3}He: Metastability-Exchange Optical Pumping (MEOP) and Spin-Exchange Optical Pumping (SEOP). Our group focuses on SEOP as MEOP polarizes gas at relatively low pressure, thus further compression is required to produce target cells.

In SEOP, alkali metal is polarized by circularly polarized laser that's tuned to the D1 transition of it. ^{3}He obtains polarization from alkali metal through spin exchange process. With the combination of hybrid alkali mixtures (typically Rb and K) and

spectrally narrowed lasers, more than 70% polarizations have been produced.

1.2   Optical pumping

1.2.1   Rb for SEOP

In optical pumping, Rb is often the alkali metal that's optically pumped by circularly polarized laser light. The angular momentum of a polarized photon is transfered to the valence electron of Rb atom. In the case of hybrid mixture of Rb/K, Rb is still the alkali metal that's pumped by laser light directly while K serves as a more efficient medium to transfer the polarization from Rb to ^{3}He compared to direct transfer from Rb to ^{3}He. Rb is so widely used mainly for its low melting point, the relative ease of acquiring laser at the Rb D1 line wavelength and the clear seperation between D1 (794.7nm) and D2 line (780nm).

The Rb melting point is at 39.5°C, so it's easy to achieve enough Rb vapor without having to drive the oven temperature too high. In our lab, depending on if the cell contains pure Rb or Rb/K mixture, the oven temperature can be between 85°C to as high as 255°C. Perhaps the most used oven temperature for hybrid is 235°C which has empirically been a good temperature to produce Rb/K mixture vapor, while 85°C is enough for pure Rb.
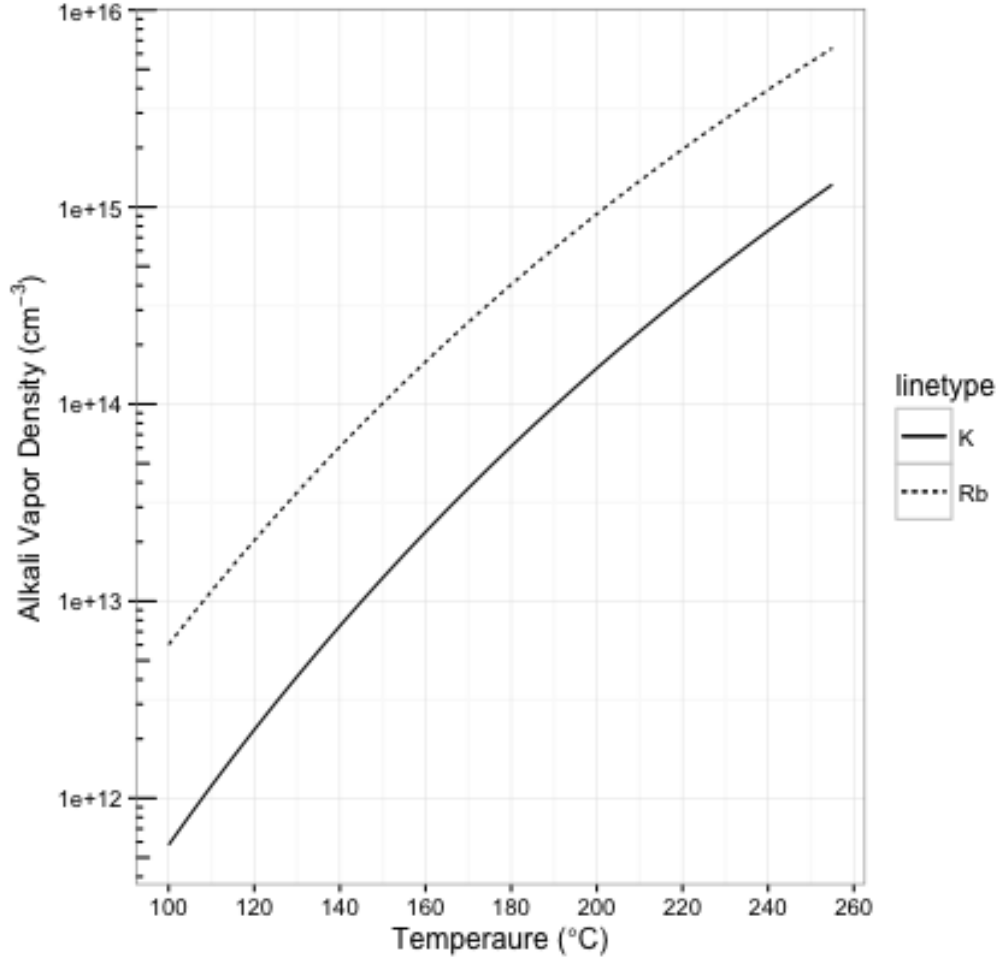
Figure 1.1: Rb And K Number Density Curves

1.2.2 Energy Levels of Alkali Metal in External Magnetic Field

The Hamiltonian for ground state (L=0) alkali metal atoms in external magnetic field is:

$$\mathbf{H} = A\mathbf{I} \cdot \mathbf{S} + g_e \mu_B S_z B_z + g_N \mu_N I_z B_z \tag{1.1}$$

3

The first term $A\mathbf{I} \cdot \mathbf{S}$ describes the coupling of the nuclear spin $\mathbf{I}$ with the electron spin $\mathbf{S}$ and is key to spin exchange, where A is the isotropic magnetic-dipole coupling coefficient. The resulting energy levels are referred to as hyperfine structure. The second and third terms describe the Zeeman splitting due to the presence of a weak external magnetic field. $\mu_B = 9.274 \times 10^{-24} J/T$ and $\mu_N = 5.051 \times 10^{-27} J/T$ are the bohr and nuclear magnetons. $g_e \approx 2$ and $g_N \approx 5.59$ are the electronic and nuclear Lande g-factors.

The linear relationship between energy levels and magnetic field only holds for weak magnetic fields as is the case with our lab where 13 Gauss is used most of the time. When the Zeeman splitting grows relative to the hyperfine energy difference one would have to take into account the quantum mixing of the states, the result is described by Breit-Rabi Formula. With 13 Gauss, the hyperfine term dominates the total Hamiltonian. The energy levels of ^{87}Rb are shown in figure **??**.
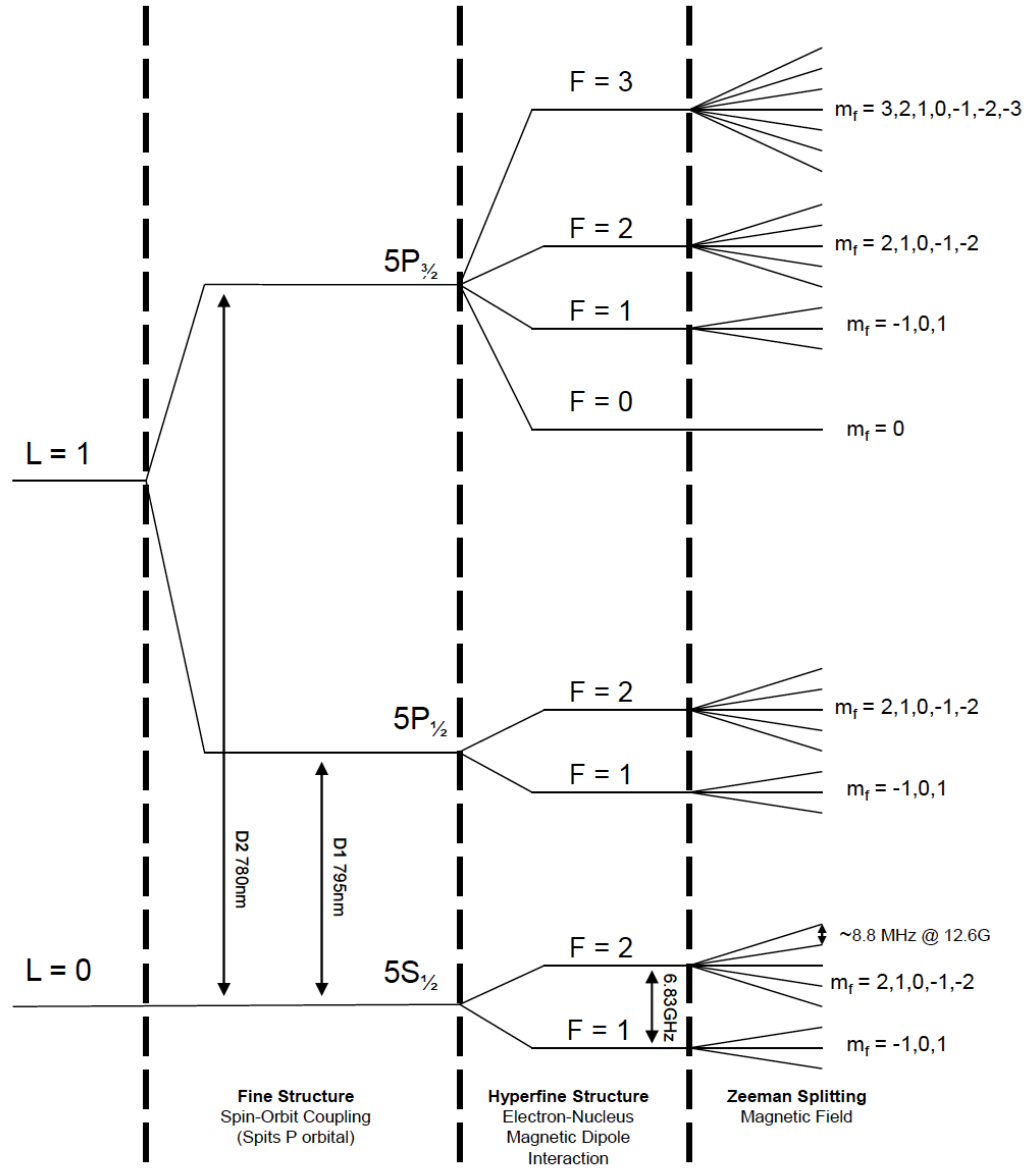
Figure 1.2: Level Diagram of ^{87}Rb. The splittings are not to scale. Adapted from Dolph's PhD thesis.

1.2.3 Optical Pumping Process Overview

For simplicity, the following discussion will ignore the nuclear spins for now. The inclusion of nuclear spins will increase the number of energy states but the optical pumping mechanism remains the same. In our typical setup, circularly polarized laser light is tuned to the D1 line of Rb and excites valence electrons of Rb from $5S_{1/2}$ state to $5P_{1/2}$ state as shown in figure 1.3 ($2S_{1/2}$ and $2P_{1/2}$ states are used in the figure for the simple model described below).

Figure 1.3: The interaction of alkali-metal atoms with left-circularly (σ^+) polarized light. (from Ref. [?])

Although left-circularly polarized light is assumed in the figure, either circular polarization works the same. Conservation of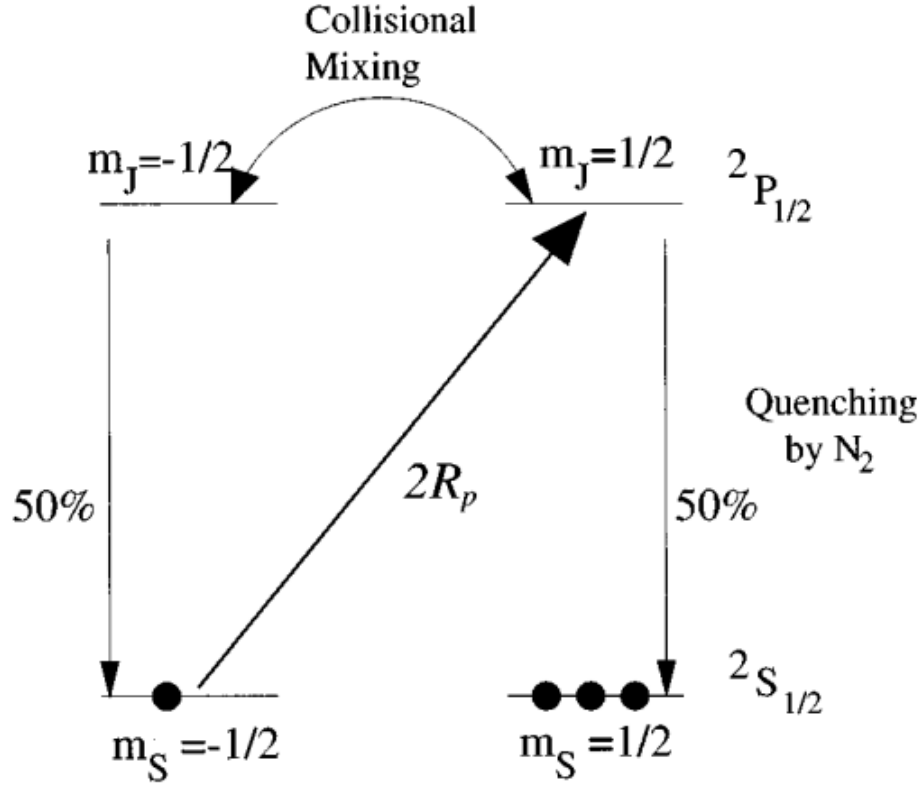 angular momentum requires $\Delta m = +1$ as the figure show. Through collisions with other Rb atoms, excited electrons will be mix and evenly distribute on the two $2P_{1/2}$ states. Electrons then decay to the two ground states with equal probabilities. The selection rule for the decay process is $\Delta m = 0$ or ± 1. Even though both grounds receive electrons from the decay, only the m = -1/2 state absorb the circular polarized photons, so atoms are in effect pumped to the m = +1/2 state. When we consider Rb with nuclear spins, both $5S_{1/2}$ and $5P_{1/2}$ states are split into more energy levels, but the net effect is still that the ground state with highest m accumulate atoms from those with lower m.

When the excited electrons decay back to the ground state, they emit unpolarized photons which can depolarize the gas. A small amount of N_2 gas is added into the cell (typically around 0.1 Amagats) to non-radiatively quench the excited electrons as N_2 molecules can absorb the released energy of spontaneous decays into their rotational and vibrational modes of oscillation. With an appropriate amount of N_2, the photon-emitting decays can be reduced to less than 5%.

1.2.4 Optical Pumping Rate

The optical pumping rate at position $\vec{r}$ can be described by

$$R = \int \Phi(\nu, \vec{r})\sigma(\nu)d\nu \tag{1.2}$$

where $\Phi(\nu, \vec{r})$ is the position dependent photon spectral flux density and $\sigma(\nu)$ is the photon absorption cross section. The cross section has a natural Lorentzian

lineshape which is broadened by Doppler effect and pressure broadening. The pressure broadening effect dominates the lineshape as our cells normally have densities well above one amagat. $\sigma(\nu)$ follows the sum rule:

$$\int \sigma(\nu)d\nu = \pi r_0 cf \tag{1.3}$$

where $r_0 = 2.82 \times 10^{-13}$ cm is the classical electron radius and f=0.337is the transition oscillator strength. Thus the photon absorption cross section can be described by Lorentzian lineshape:

$$\sigma(\nu) = fr_e c\frac{\frac{\Gamma_A}{2}}{(\nu - \nu_0)^2 + (\frac{\Gamma_A}{2})^2} \tag{1.4}$$

where Γ_A is the pressure dependent FWHM. At the front of the cell, the photon spectral flux density is the product of a Gaussian spatial distribution and a Gaussian spectrum.

$$\phi(\nu, \vec{r}) = \phi_0(\vec{r})G(\nu) \tag{1.5a}$$

$$\phi_0(\vec{r}) = \frac{P}{h\nu}\frac{2}{\omega^2\pi}e^{2r^2/\omega^2} \tag{1.5b}$$

$$G(\nu) = \frac{1}{\sqrt{2\pi}\sigma_l}e^{-(\nu-\nu_l)^2/2\sigma_l^2} \tag{1.5c}$$

where P is the laser power; ω is the beam waist; σ_l is the Gaussian width of the laser and ν_l is the central laser frequency.
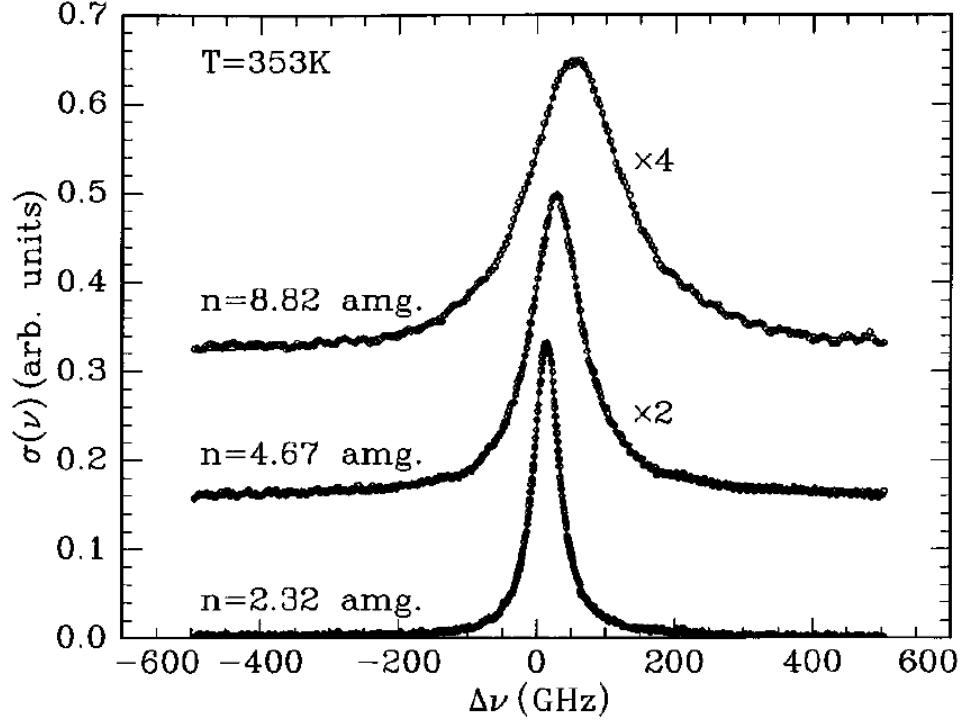
Figure 1.4: Absorption cross section for Rb D_1 line in the presence of three different densities of ^{3}He. (from Ref. [1])

1.2.5 Polarization Time Evolution

Although polarizations of Rb electrons are more complex, ^3He nuclei have an intrinsic nuclear spin of 1/2, and it's simpler to explain the math with spin of 1/2, let's define the polarization as the asymetry between +1/2 state and -1/2 state:

$$P = \frac{\rho_{+1/2} - \rho_{-1/2}}{\rho_{+1/2} + \rho_{-1/2}} = \rho_{+1/2} - \rho_{-1/2} \qquad (1.6)$$

where $\rho_{\pm 1/2}$ is the population in the $\pm 1/2$ state.

The time evolution of polarization for both Rb electrons and ^3He follows the equation:
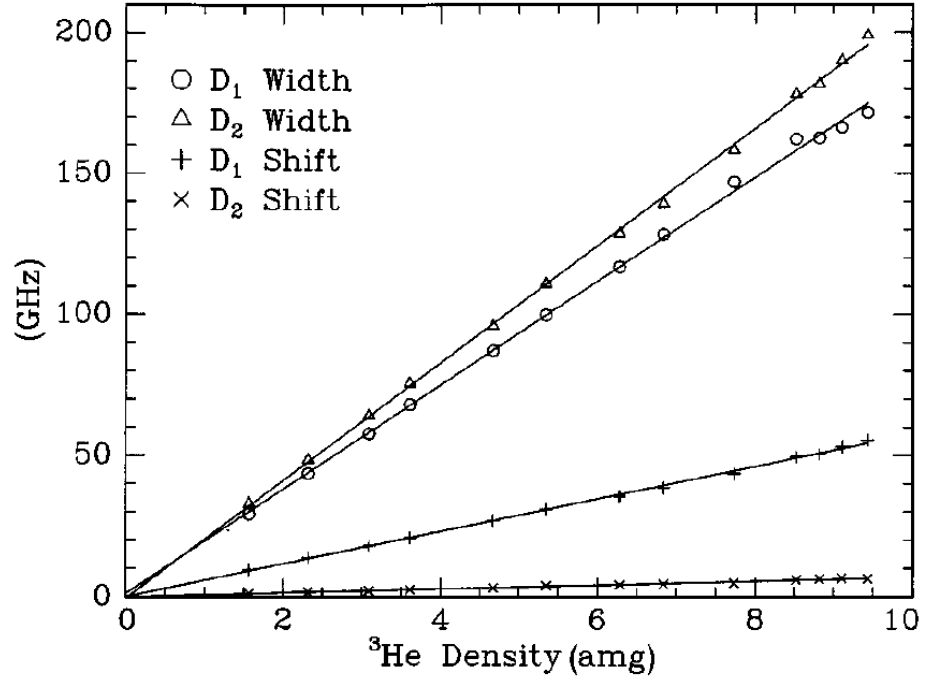
Figure 1.5: The shift and the broadening due to presence of ^3He for Rb D_1 and D_2 lines. (from Ref. [1])

$$\frac{dP}{dt} = \gamma(1 - P) - \Gamma \cdot P \qquad (1.7)$$

γ is the polarization rate and Γ is the depolarization rate in the above differential equation. The solution has the simple form of:

$$P(t) = Ce^{-(\gamma+\Gamma)t} + \frac{\gamma}{\gamma + \Gamma} \qquad (1.8)$$

Note the depolarization rate also contributes to the speed at which P approaches saturation. The saturated polarization is defined as the value of P in the limit t $\rightarrow \infty$:

10

$$P_\infty = \frac{\gamma}{\gamma + \Gamma} \tag{1.9}$$

The initial polarization is defined as the value of P at t = 0:

$$P_0 = C + \frac{\gamma}{\gamma + \Gamma} = C + P_\infty \tag{1.10}$$

Thus, P(t) can be expressed as:

$$P(t) = (P_0 - P_\infty)e^{-(\gamma + \Gamma)t} + P_\infty \tag{1.11}$$

In the case of polarizing Rb with a pump laser. γ is the pumping rate R and Γ is the Rb spin relaxation rate Γ_{Rb}. There is typically a small angle θ between the pump laser and the magnetic field that separates the different spin states of Rb valence electrons even though great effort has been made to minimize the angle. Thus P(t) can be rewritten as:

$$P(t) = P_0 e^{-(R + \Gamma_{Rb})t} + P_{laser} cos\theta \frac{R}{R + \Gamma_{Rb}}(1 - e^{-(R + \Gamma_{Rb})t}) \tag{1.12}$$

P_{laser} is the circular polarization of the pump laser which is above 99.5%. Rb close to the front side of the cell can reach above 97% (depends on the laser power and other factors) on the order of 100's of microseconds. As the laser propagates through the cell, power is attenuated by Rb vapor. Therefore Rb polarization at the back side of the cell is lower than that at the front side. One way to overcome the problem is to shine pump laser from both sides of the side which would lead to higher overall Rb polarization and ^{3}He polarization.

Spins are thermally polarized with the presence of a magnetic field even without external pumping source. The probability for a spin to be in state s is:

$$Prob. = \frac{e^{-E_s/k_B T}}{\sum_{si} e^{-E_{si}/k_B T}} \tag{1.13}$$

where E_s is the energy of the state, k_B is the Boltzmann constant and T is the temperature. Using the thermal distribution, under typical operating conditions, ^3He polarization is 10^{-9} and Rb polarization is 10^{-5}. Both are negligible without active pumping.

1.2.6 Rb Spin Destruction Rate

There are two main mechanisms of Rb depolarization: the binary collisions with Rb, ^{3}He and N_2 and the formation and breakup of van der Waals molecules, while the second mechanism is negligible for ^{3}He cells. The Rb spin destruction rate can then be expressed as

$$\Gamma_{Rb} = k_{Rb-Rb}[Rb] + k_{Rb-^3He}[^3He] + k_{Rb-N_2}[N_2] \tag{1.14}$$

where k_{Rb-X} is the spin destruction rate constant and [X] is the density of X. Dolph has summarized these constants based on measurements from various groups:

$$k_{Rb-^3He}(T) = 55.9(9) \left(\frac{T}{473.15K} \right)^{3.31(12)} Hz/amg \tag{1.15a}$$

$$k_{Rb-N_2}(T) = 290(30) \left(\frac{T}{473.15K} \right)^{2.0(25)} Hz/amg \tag{1.15b}$$

$$k_{Rb-Rb} = 4.813(48) \times 10^{-13} Hz \cdot cm^3 \tag{1.15c}$$

For a pure Rb cell at 170°C with the following densities in the pumping chamber:

$$[^3He] \approx 8.0 amg \tag{1.16a}$$

$$[N_2] \approx 0.08 amg \tag{1.16b}$$

$$[Rb] \approx 6.0 \times 10^{14} cm^{-3} \tag{1.16c}$$

The approximate spin destruction rates due to various gases are:

$$\Gamma_{Rb-^3He} \approx 360 Hz \tag{1.17a}$$

$$\Gamma_{Rb-N_2} \approx 20 Hz \tag{1.17b}$$

$$\Gamma_{Rb-Rb} \approx 289 Hz \tag{1.17c}$$

The total spin destruction rate is 669 Hz.

1.3 Spin Exchange

Following equation 1.12, the time evolution of ^3He polarization can be expressed as:

$$P_{^3He}(t) = P_0 e^{-(\gamma_{se}+\Gamma)t} + P_{Rb}\frac{\gamma_{se}}{\gamma_{se} + \Gamma}(1 - e^{-(\gamma_{se}+\Gamma)t}) \tag{1.18}$$

The saturation polarization is

$$P_\infty = P_{Rb}\frac{\gamma_{se}}{\gamma_{se} + \Gamma} \tag{1.19}$$

where γ_{se} is the spin exchange rate between ^{3}He and Rb, and Γ is the spin relaxation rate.

1.3.1 Spin-Dependent Interactions

The key process in spin-exchange optical pumping is collisional transfer of polarization between optically pumped alkali-metal atoms and the nuclei of the noble gas atoms. As in Fig. 1.7, the transfer of angular momentum occurs either while the atoms are bound in van der Waals molecules or in simple binary collisions. For ^3He, binary collisions dominate, and the contribution from van der Waals molecules is negligible. The time scale for binary collisions is on the order of 10^{-12} sec, so the collision can induce both $\Delta F = \pm 1$ and $\Delta F = 0$ transitions between hyperfine sublevels. For heavier noble gases like ^{129}Xe at pressure of a few tens of Torr, the contributions of van der Waals molecuels can greatly exceed that of binary collisions. At several atms which is the typical operating pressure for SEOP, the time scale of van der Waals molecules is greatly limited by collision so that the binary collisions dominate.

Spin-dependent interactions produce the spin transfer and relaxation. For SEOP, spin-rotation interaction between $\vec{S}$ and the rotational angular momentum $\vec{N}$ and the isotropic hyperfine interaction between $\vec{S}$ and the noble-gas nuclear spin $\vec{I}$ dominate the spin-exchange process:

$$V_1(\vec{R}) = \gamma(R)\vec{N} \cdot \vec{S} + A(R)\vec{I} \cdot \vec{S} \qquad (1.20)$$

$\vec{I_a}$ and $\vec{I_b}$ are the nuclear spins of the atomic pair.

The spin-rotation interaction is caused by the magnetic fields from relative motion of the charges of the colliding atoms, and the isotropic hyperfine interaction comes from the magnetic field inside the nucleus of the noble-gas atom.

An alkali-metal atom and a noble-gas atom interact via both a large spin-independent
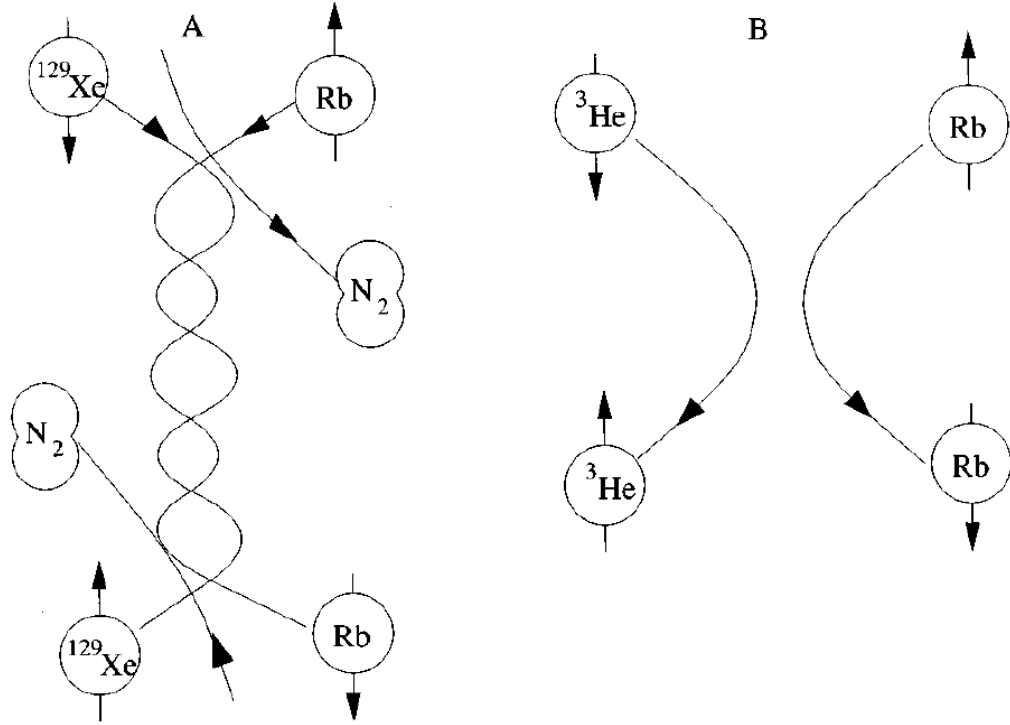
Figure 1.6: A. Formation and breakup of alkali-metal/noble-gas van der Waals molecule. B. Binary collision between an alkali-metal atom and a noble-gas atom. (from Ref. [?])

interaction $V_0(R)$ and a small spin-dependent interaction $V_1(R)$. At the high operating temperatures, V_0 determines classical collision trajectories, while V_1 acts as a small perturbation. We'll focus on V_1 below since it is responsible for spin exchange.

Including a few more terms that were neglected in Eq. 1.20, the spin-dependent interaction $V_1(R)$ can be expressed as:

$$V_1(\vec{R}) = \gamma(R)\vec{N} \cdot \vec{S} + \sum_k A_k(R)\vec{I}_k \cdot \vec{S}$$

$$+ \sum_k B_k(R)\vec{I}_k \cdot (3\vec{R}\vec{R} - 1) \cdot \vec{S} \qquad (1.21)$$

$$+ \sum_k C_k(R)\vec{I}_k \cdot (3\vec{R}\vec{R} - 1) \cdot \vec{I}_k$$
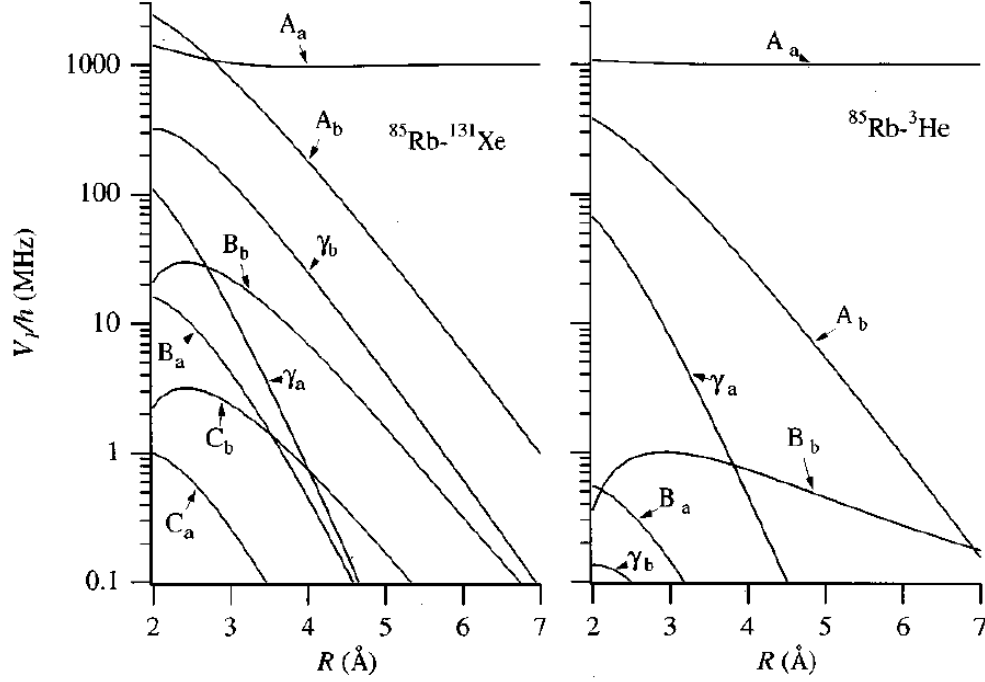

Figure 1.7: Strengths of various spin-dependent interactions as functions of separation(from Ref. [?])

where γ is the coefficient of the spin-rotation interaction, while A_k, B_k, C_k are the coefficients for isotropic magnetic-dipole hyperfine interactions, anisotropic magnetic-dipole hyperfine interactions, and electric quadrupole interactions, respectively. A_a

16

greatly exceed other coefficients as the separations between atoms increase.

The isotropic hyperfine interactions come from the Fermi-contact magnetic fields of the nuclei pair.

$$A_b(R) = \frac{8\pi g_s \mu_B \mu_b}{3I_b} |\eta\phi_0(R)|^2 \tag{1.22}$$

where η is the enhancement factor which equals to the ratio of the perturbed wave function at the noble gas nucleus to that without the noble gas atom. The isotropic hyperfine interaction also introduces a frequency of the magnetic resonance lines for alkali-metal and noble gas atoms. The frequency shift of alkali-metal electrons due to the polarized noble gas nuclei is used in the technique Electron Paramagnetic Resonance (EPR) to calculate the polarization of noble gas nuclei.

The isotropic magnetic-dipole coupling polarizes the noble gas nuclei parallel to the electron spin polarization, while the anisotropic magnetic-dipole coupling polarizes in the opposite direction. Fortunately, the anisotropic interaction is negligible compared to isotropic interaction.

1.3.2   Spin Exchange Rate

The spin exchange rate due to binary collisions is:

$$\gamma_{se} = <\sigma_{se}v> [Rb] = k_{se}[Rb] \tag{1.23}$$

where $k_{se} = <\sigma_{se}v$ is the velocity-averaged spin exchange rate constant. k_{se} for spin exchange between ^3He and Rb is:

$$k_{se}^{^3He-Rb} = (6.7 \pm 0.7) \times 10^{-20} cm^3/s \tag{1.24}$$

Under 170°C which is a typical temperature that we run tests with,

$$[Rb] = 2.60 \times 10^{14} cm^{-3} \tag{1.25}$$

Thus for a single chamber cell,

$$frac1\gamma_{se} \approx 15.9 hrs \tag{1.26}$$

1.4 ^3He Spinup and Relaxation

Similar to the optical pumping process of Rb, ^3He polarization can be described by

$$P_{^3He}(t) = P_0^{^3He} e^{-(\gamma_{se}+\Gamma)t} + P_\infty^{^3He}(1 - e^{-(\gamma_{se}+\Gamma)t}) \tag{1.27}$$

where the saturation polarization is

$$P_\infty^{^3He} = P_\infty^{Rb} \frac{\gamma_{se}}{\gamma_{se} + \Gamma} \tag{1.28}$$

And Γ is the total relaxation rate of ^{3}He nucleus spin polarization,

$$\Gamma = \Gamma_{dipolar} + \Gamma_{inhomogeneity} + \Gamma_{wall} \tag{1.29}$$

When a target cell are used in electron scattering experiments where an electron beam goes through part of the cell, an additional relaxation rate due to the beam Γ_{beam} should also be included.

The coupling of nuclear spin to orbital angular momentum creates an intrinsic ^{3}He relaxation rate that depends on density. At room temperature ($23°C$), the dipolar relaxation rate is

$$\frac{1}{\Gamma_{dipolar}} = \frac{[^3He]}{744} hr^{-1} \tag{1.30}$$

where $[^3He]$ is the ^3He density in amagats. Assuming the cell density is 8 amg, the relaxation rate is $1/93$ hr^{-1}. In addition, there is an additional intrinsic relaxation due to the spin-rotation interaction. This mechanism dominates the relaxation for ^{129}Xe but is small for ^{3}He.

The relaxation rate due to field inhomogeneities is

$$\Gamma_{inhomogeneity} = D\frac{|\nabla B_x|^2 + |\nabla B_y|^2}{B_0^2} \tag{1.31}$$

where D is the ^{3}He diffusion constant, ∇B_x and ∇B_y are the transverse magnetic field inhomogeneities, B_0 is the holding field along z-axis. Under operating conditions, assuming the pressure is around 12 atm and field is 12.6 G, $D \approx 0.16 cm^2/s$ and the field inhomogeneities are 10mG/cm, the relaxation rate is 1/1400 hr^{-1}

Wall relaxation is typically the dominant relaxation mechanism for cells in our lab. This mechanism depends on the property of the inner surface of glass. Most of the target cells are contructed with reblown General Electric Type 180 (GE-180) glass. This aluminosilicate glass is highly impermeable to ^{3}He. The wall relaxation is believed to be associated to several different mechanisms, such as paramagnetic impurities in the glass and microfissures in the surface that could trap ^{3}He atoms. It has been found reblowing the glass can help lower the wall relaxation rate because it

reduces the number of microfissures. The wall relaxation is not well understood, but it is believed to scale with the surface-to-volume ratio:

$$\Gamma_{wall} = \rho S/V \tag{1.32}$$

where ρ is called relaxivity.

1.5 X Factor

In 2006, Babcok *et al.* reported evidence of a previously unrecognized spin relaxation mechanism, and named it X factor. This mechanism appears to be temperature dependent and roughly proportional to alkali density. The X factor limits the maximally achievable ^{3}He polarization even with infinite laser power. The saturation polarization is

$$P_\infty^{^3He} = P_\infty^{Rb} \frac{\gamma_{se}}{\gamma_{se}(1+X)+\Gamma} \tag{1.33}$$

In the presence of infinite laser power where $\gamma_{se} \gg \Gamma$, the saturation polarization becomes

$$P_\infty^{^3He} = P_\infty^{Rb} \frac{1}{1+X} \tag{1.34}$$

Chapter 2

^{3}He Polarimetry

2.1 Overview

Traditional pure glass target cells are studied mainly using Adiabatic Fast Passage (AFP) Nuclear Magnetic Resonance (NMR) and Electron Paramagnetic Resonance (EPR). AFP is a technique that allows us to monitor a signal that's directly proportional to the $3He$ polarization, which then provides a means to gain knowledge of properties of cell including pumping time and relaxation rates. The EPR technique utilizes the fact that polarized ^{3}He produces frequency shift of the magnetic resonance lines of alkali metal to measure the ^{3}He polarization. When AFP and EPR are combined, we can calculate the calibration constant between AFP signal and ^{3}He polarization.

A significant focus of my studies is on exploring cells that incorporate metal. Unfortunately, AFP is not suitable for studying these cells as it requires exposing the entirety of the cell to a Radio Frequency magnetic field in an attempt to flip all spins

in the cell. For these cells, Pulsed Nuclear Magnetic Resonance (PNMR) has proven to be very useful. PNMR only applies a pulsed RF field to a small selected part of the cell which makes it relatively easy to prevent metal from distorting the signal. However, the spins tipped by applying the pulse lose their transverse component (which depends on the "tip angle"), we typically allow some time for this portion of gas to diffuse out of the region before taking the next measurement on a fresh sample of the gas. The rate at which measurements are taken is limited by this requirement.

This chapter introduces the three techniques mentioned above and how they're used for our studies.

2.2 Adiabatic Fast Passage

2.2.1 Nuclear Magnetic Resonance

The energy of a magnetic moment in an external field is

$$E = -\vec{\mu} \cdot \vec{B}_0 = -\mu_z B_0 \tag{2.1}$$

where $\vec{\mu}$ is the magnetic moment, for a spin-1/2 nuclei, the energy is

$$E = -\gamma B_0 \hbar/2 \tag{2.2}$$

γ is the gyromagnetic ratio, $\gamma/2\pi \approx 3.2434 kHz/Gauss$. When a oscillating magnetic field with the frequency $\omega = \gamma B_0$ is present, transitions between the +1/2 and -1/2 states are induced. This frequency is called Larmor frequency. When a nucleus is placed in an external magnetic field that is not aligned with its magnetic moment,

it will precess at the Larmor frequency.

2.2.2 The Rotating Coordinate System

2.2.2.1 Classical Formulation

For a nucleus in an external field $\vec{B}$ with $\gamma\hbar\vec{I}$ as its nuclear angular momentum, the equation of motion in a stationary coordinate system is [?]

$$\hbar\frac{d\vec{I}}{dt} = \gamma\hbar\vec{I} \times \vec{B} \tag{2.3}$$

Let $\frac{\partial}{\partial t}$ represent the derivative with respect to a coordinate system that rotates with angular velocity $\vec{\omega}$,

$$eq2\frac{d\vec{I}}{dt} = \frac{\partial\vec{I}}{\partial t} + \vec{\omega} \times \vec{I} \tag{2.4}$$

Substitute Eq.?? into Eq.??, $\vec{I}$ in the rotating frame satisfies the equation of motion

$$\hbar\frac{\partial\vec{I}}{\partial t} = \gamma\hbar\vec{I} \times (\vec{B} + \vec{\omega}/\gamma) = \gamma\hbar\vec{I} \times \vec{B_{eff}} \tag{2.5}$$

where $\vec{B_{eff}}$ is the effective field in the rotating frame

$$\vec{B_{eff}} = \vec{B} + \vec{\omega}/\gamma \tag{2.6}$$

Thus, for an observer in the rotating frame, the net effect is the same as changing the field to include an additional term ω/γ.

If we apply this result to rotating magnetic fields, we will get the core idea of performing an Adiabatic Fast Passage (AFP) measurement. Assuming a constant

23

field $\vec{B}$ and another field $\vec{B_1}$ perpendicular to $\vec{B}$ and rotates with angular velocity $-\omega$. In the rotating frame that rotates with $\vec{B_1}$, both aforementioned field are constant. The effective field in the rotating frame is

$$B_{eff}\vec{z} = (B - \omega/\gamma)\vec{z} + B_1\vec{x'} \tag{2.7}$$

where $\vec{x'}$ is the direction that $\vec{B_1}$ is in. When on resonance ($B = \omega/\gamma$), the effective field is perpendicular to the constant field $\vec{B}$.

2.2.2.2 Quantum Mechanical Formulation

The Shrödinger equation for a magnetic moment in an external field is

$$i\hbar\dot{\psi} = \mathcal{H}\psi = -\gamma\hbar\vec{I}\cdot\vec{B}\psi \tag{2.8}$$

Let ψ and $\vec{B}$ be the wave function and magnetic field in a stationary frame and ψ_r and $\vec{B_r}$ be the same quantities in a rotating frame with angular velocity $\vec{\omega}$. Using the rotation operator in quantum mechanics,

$$\psi = e^{-i\vec{\omega}\cdot\vec{I}t}\psi_r \tag{2.9a}$$

$$\vec{I}\cdot\vec{B_r} = e^{i\vec{\omega}\cdot\vec{I}t}\vec{I}\cdot\vec{B}e^{-i\vec{\omega}\cdot\vec{I}t} \tag{2.9b}$$

Substituting 2.8 into Eq.2.8, the Shrödinger equation in the rotating frame is obtained

$$i\hbar\dot{\psi}_r = -\gamma\hbar\vec{I}\cdot(\vec{B_r} + \vec{\omega}/\gamma)\psi_r = -\gamma\hbar\vec{I}\cdot\vec{B_{eff}}\psi_r \tag{2.10}$$

24

The same effective field in the rotating frame is reached as that from the classical derivation.

2.2.3 Adiabatic Fast Passage

Adiabatic Fast Passage (AFP) NMR is used to measure the ^{e}He polarization. In an AFP measurement, with the assistance of a oscillating radiofrequency (RF) field, the spins follow the effective field in a rotating frame (as discussed in more detail below) and are flipped 180 degrees to the opposite direction and then flipped back, producing two peaks in signal when they're perpendicular to the pick up coils.

The flipping process can be achieved by either sweeping the main holding field or sweeping the RF frequency so that the longitudinal component of effective field in the rotating field goes through zero. AFP measurements in out lab are typically done by sweeping the holding field while keeping the RF frequency constant. The RF coils produce a RF field of magnitude $2B_1$ perpendicular to the main holding field B. The oscillating field has a frequency of ω and can be decomposed into two counter-rotating components with the same amplitude B_1. Only the component rotating in direction to be able to give a resonance in Eq.2.7 has an important effect. In this frame, the effective field is

$$B_{eff}\vec{z} = (B - \omega/\gamma)\vec{z} + B_1\vec{x'} \tag{2.11}$$

as discussed above. The other rotating component does not affect the spins. In an AFP measurement, the holding field starts from a value that's lower than ω/γ ($\omega/\gamma - B \gg B_1$), so that the effective field is almost aligned with the holding field

(and the spins). The holding field is then swept at a constant rate through resonance to a value greater than ω/γ. The sweeping rate is of great importance. The sweep needs to be slow enough so that the nuclear spins can follow the effective field

$$\frac{\dot{B}}{B_1} \ll \omega \tag{2.12}$$

Sweep that satisfies this condition is considered as adiabatic.

Bibliography

[1] E. M. M. V. Romalis and G. D. Cates. Pressure broadening of rb d_1 and d_2 lines by ^{3}he, ^{4}he, n_2, and xe: line cores and near wings. *Phys. Rev. A*, 56(6), 1997.

Appendix A

Appendix title

This is Appendix A.

You can have additional appendices too (*e.g.*, `apdxb.tex`, `apdxc.tex`, *etc.*). If you don't need any appendices, delete the appendix related lines from `thesis.tex` and the file names from `Makefile`.